ACS OMEGA

http://pubs.acs.org/journal/acsodf

Article

Monitoring and Prediction of Horizontal Displacement of Underground Enclosure Piles in Subway Foundation Pits

Yue Dong, Yuanzhong Luan, Fei Wang, Huilong Yang, Zheng Jia, and Hengxuan Luan*

Cite This: *ACS Omega* 2023, 8, 23389−23400

Read Online

ACCESS | Metrics & More | Article Recommendations

ABSTRACT: Urban rail transportation and underground space development and utilization are initiatives to solve urban traffic congestion. The monitoring and prediction of the stability of underground enclosure piles in foundation pits is a key index for the dynamic evaluation of the stability of underground space engineering. In this paper, we focused on the problem that the dynamic prediction accuracy and stability of foundation pit retaining piles in the Qingdao area are not high. Based on the analysis of various time function curves and the physical meaning of the parameters, we proposed the Adjusted-Logistic time function model, which introduces three physical parameters to adjust the deformation velocity and deformation acceleration in different stages for better accuracy. It could predict the deformation process of underground enclosure piles under different geological engineering conditions. It was verified in the field that the root-mean-square error (RMSE) of the Adjusted-Logistic function was 0.5316, MAE was 0.3752, and R^2 was 0.9937, which were better than those of Gompertz, Weibull, and Knothe time function models. Meanwhile, it showed that with the increase of excavation depth, the maximum horizontal displacement of the underground enclosure piles gradually decreased and finally stabilized at 0.62−0.71 H. We established a catastrophe model of the horizontal displacement cusp at the observation point of the underground enclosure piles by using the time series of the measured data. It could determine the weak location of the underground enclosure pile stability and realize the multipoint warning of the foundation pit stability, which would ensure safe construction.

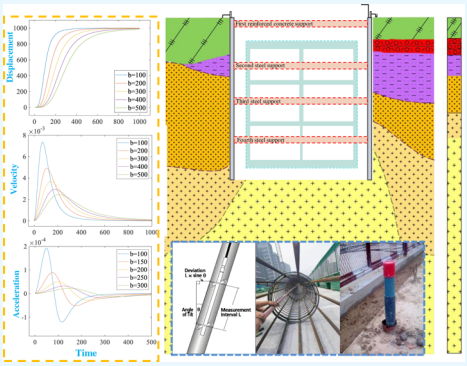

1. INTRODUCTION

The rapid economic development of cities urgently requires the excavation of subway tunnels near or under existing buildings.[1] One of the most important tasks of metro construction is the excavation and construction of station pits. In particular, most of the subway stations are located in flourishing urban areas with deep pits, dense surrounding buildings, and complicated underground pipeline networks.[2] The excavation of subway station pits easily disturbs the surrounding soil[3] and changes the soil stress field[4] and displacement field,[5] which is very likely to cause secondary disasters such as underground pipe network damage, surface building tilt, cracks, and even collapse.[6−8] At present, the popular precautions and regulations to reduce disaster risk are increasing the underground enclosure piles during excavation, which would reduce the deformation of surrounding strata and impact on surface buildings.[9] Therefore, carrying out stability monitoring and dynamic risk warning of underground enclosure piles is a key issue to ensure the safety of foundation pits, guarantee the implementation of underground space engineering, and achieve rapid urban development.[10]

Both domestic and international scholars have unveiled the deformation law of the foundation pit. In the 1940s, Peck and Terzaghil established the total stress calculation method for predicting slope stability and internal support load magnitude.[11] In 1993, Ou discovered that there is a quantitative relationship between the maximum horizontal displacement of the enclosure structure and the excavation depth and that the ratio between the maximum settlement value of the ground surface and the deformation value of the enclosure structure falls within a specific range.[12] In the study of the unloading modulus of typical soft soil in Shanghai, Qin and Hu[13] found that the stress−strain relationship of soft soil is closely related to the stress path and its unloading stress−strain relationship is in the form of a hyperbola. They also obtained the formula of the tangential unloading modulus of soil. In 2007, Xu concluded that the maximum horizontal movement of a subsurface diaphragm wall was between 0.1% and 1%H, by assessing a number of foundation pit projects with the subterranean diaphragm wall enclosure technology in the

Received: January 3, 2023
Accepted: May 31, 2023
Published: June 21, 2023

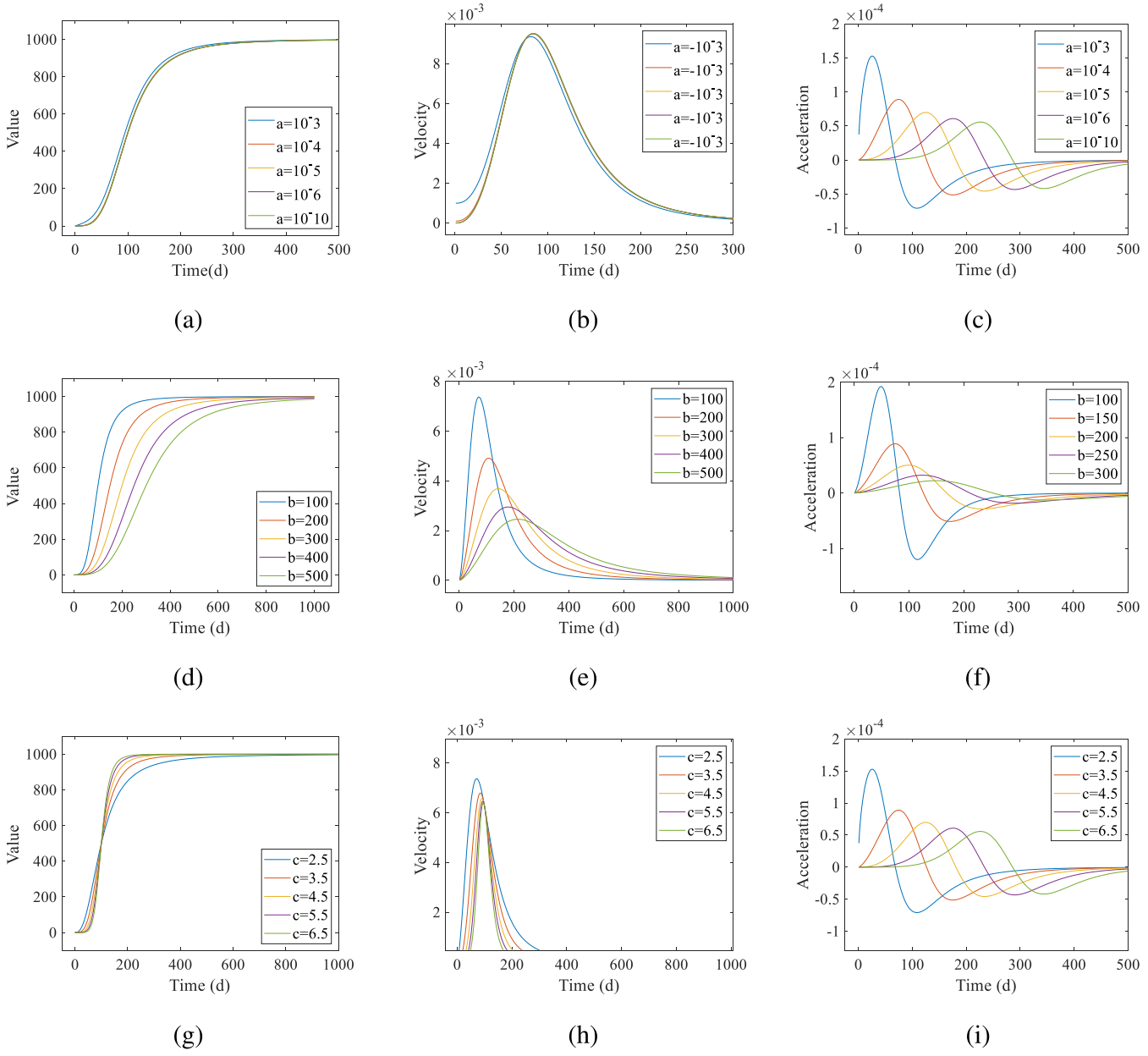

Figure 1. Relationship between the Adjusted-Logistic function curve and parameters *a*, *b*, and *c*. (a) Relationship between value curve and parameter *a*; (b) relationship between the velocity curve and parameter *a*; (c) relationship between the acceleration curve and parameter *a*; (d) relationship between the value curve and parameter *b*; (e) relationship between the velocity curve and parameter *b*; (f) relationship between the acceleration curve and parameter *b*; (g) relationship between the value curve and parameter *c*; (h) relationship between the velocity curve and parameter *c*; and (i) relationship between the acceleration curve and parameter *c*.

Shanghai area.[14] Yang and Zhong[15] used FLAC3D to numerically simulate a typical foundation excavation example in Tianjin and clarified the soil rebound at the bottom of the pits and the spatial and temporal effects of engineering pile bearing under the excavation unloading conditions in Tianjin. In 2015, Liao et al. analyzed the deformation law of foundation pits with different structures and shapes of enclosure structures.[16] In 2018, Liu et al. proposed the active control theory of lateral deformation of enclosure structures.[17] Liu simulated the deformation law of foundation pit excavation on an underground diaphragm wall, ground surface, and surface building by means of finite elements.[18] However, there are fewer studies on the deformation law of foundation pits under the geological conditions of the upper soft and lower hard, typical water bearing sandy ground in Qingdao.

The prediction model is based on mechanical theory to predict the maximum deformation and explore the distribution of the maximum deformation, but it cannot represent the changing process of the elastic pile in the time dimension.[19] Foundation pit construction is a dynamic process, and the induced deformation of elastic piles increases over time until it eventually stabilizes. In the past few decades, scholars at home and abroad have conducted a lot of research on the time function of dynamic prediction. The Polish scholar Knothe[20] derived the Knothe time function in 1952 and found that the sedimentation velocity was proportional to the difference between the maximum sinking value and the settlement value

https://doi.org/10.1021/acsomega.2c00582
ACS Omega 2023, 8, 23389−23400

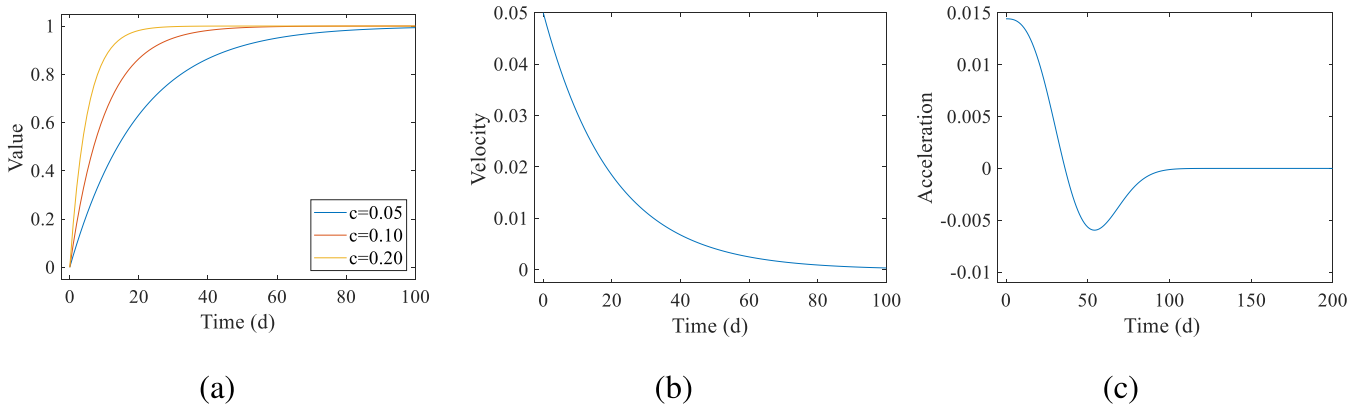

Figure 2. Curve of the Knothe function. (a) Relationship between the value curve and parameter c; (b) velocity curve; and (c) acceleration curve.

at a certain moment. Zhang and Cui[21] constructed a new segmented Knothe time function model with a wider application range and higher prediction accuracy, which expanded the applicability of its dynamic prediction and improved its accuracy in predicting the dynamic subsidence of the earth. Yu and Liu[22] established a Gompertz model for embankment settlement prediction and proved the feasibility of the model with examples. Liu et al.[23] found that the Weibull time function model realized the whole dynamic prediction of land surface subsidence. Based on the logistic growth model, Xu and Li[24] proposed a time function that can be used for surface subsidence prediction in goaf. Xi et al.[25] improved the logistic function model and established a segmented logistic function model. Li et al.[26] proposed an improved logistic time function and found that the spatiotemporal variation characteristics conformed to the actual law of surface movement. However, the previous time function model curve presents a symmetric state at the middle moment of the deformation cycle, and this law is merely applicable to the ground deformation in the ideal state. It cannot express that the foundation pit deformation is affected by groundwater, unbalanced building load, construction disturbance, and other multiconforming influences, presenting an asymmetric state. That means the previous time function model cannot achieve an accurate prediction of subway foundation pit deformation.

Taking the dynamic deformation of underground enclosure piles in the underground foundation pit of Qingdao as the main research objective, this paper analyzed the existing time function model curve and the physical significance of its parameters and established an Adjusted-Logistic time model with three parameters. The model changes the symmetry of the original model and can adjust the deformation value and deformation rate in the middle moment of the whole deformation cycle, which realizes the fitting of the asymmetric curve and is more in line with the objective deformation law. First, the Adjusted-Logistic time model is compared with the existing models by parametric experiments and theoretical analysis, and its advantages are found. Furthermore, on-site monitoring experiments were carried out to verify the effectiveness of the force−time function model through deformation data analysis. The distribution law of the maximum horizontal displacement of underground piles was proposed. And the horizontal displacement cusp mutation model was established to evaluate the stability of the subway foundation pit. It put forward suggestions for the timely reinforcement of the continuous wall of deep foundation pits and provided a reliable technical basis for the safe excavation of foundation pits of urban subway stations.

2. IMPROVED DYNAMIC PREDICTION FUNCTION

2.1. Adjusted-Logistic Function Model. The time function is time as the independent variable of the dimensionless function; the value of the domain can traverse the [0,1] interval, and it controls the function of the curve shape and change characteristics through the relevant parameters.[27] If the time function is used, $\varphi(t)$, the maximum deformation value at a point of the pit is S_{max}, the settlement at that point at a certain time is the product of and, obviously, determines the convergence value of the settlement curve but cannot affect the trend of the settlement curve.[28] In this paper, the Adjusted-Logistic time function model is established on the basis of the two parameters of the Logistic time function model, and the parameter a, which adjusts the symmetry of the function curve, is introduced, and the model expression is

$$s(t) = s_{max} \times \left[1 - \frac{e^{-at}}{1 + (b^{-1}t)^c}\right] \quad (1)$$

where S_{max} is the maximum settlement value of the surface; a, b, and c denote the time influence parameters related to the overburden lithology; and t is the time parameter in days. The curve of Adapted-Logistic time function model is shown in Figure 1.

The newly established Adapted-Logistic time function predict model is expected to have the following characteristics: (1) The value range of the time function satisfies [0,1], the function increases slowly from 0, then increases rapidly, and it reaches the maximum sink value when the surface stops deforming, at which time the function value converges to 1. (2) The sinking velocity variation represented by the time function satisfies $0 \rightarrow V_{max} \rightarrow 0$, and the sink acceleration satisfies $0 \rightarrow +a_{max} \rightarrow 0 \rightarrow -a_{max} \rightarrow 0$. (3) In this paper, a curve symmetry adjustment factor is introduced so that the Adapted-Logistic function can represent the asymmetric deformation curve. In other words, the sink acceleration at the middle moment of the whole sinking process is not necessarily zero but belongs to a variable space ($a \subseteq [0 - \mu, 0 + \mu]$, $(\mu \geq 0)$); the sinking velocity does not necessarily reach the maximum velocity but belongs to the adjustable space ($V \subseteq [V_{max} - \vartheta, V_{max} + \vartheta]$, $(\vartheta \geq 0)$). This improvement makes the time function model more practical and more consistent with the deformation law of the subway pit.

https://doi.org/10.1021/acsomega.2c00582
ACS Omega 2023, 8, 23389−23400

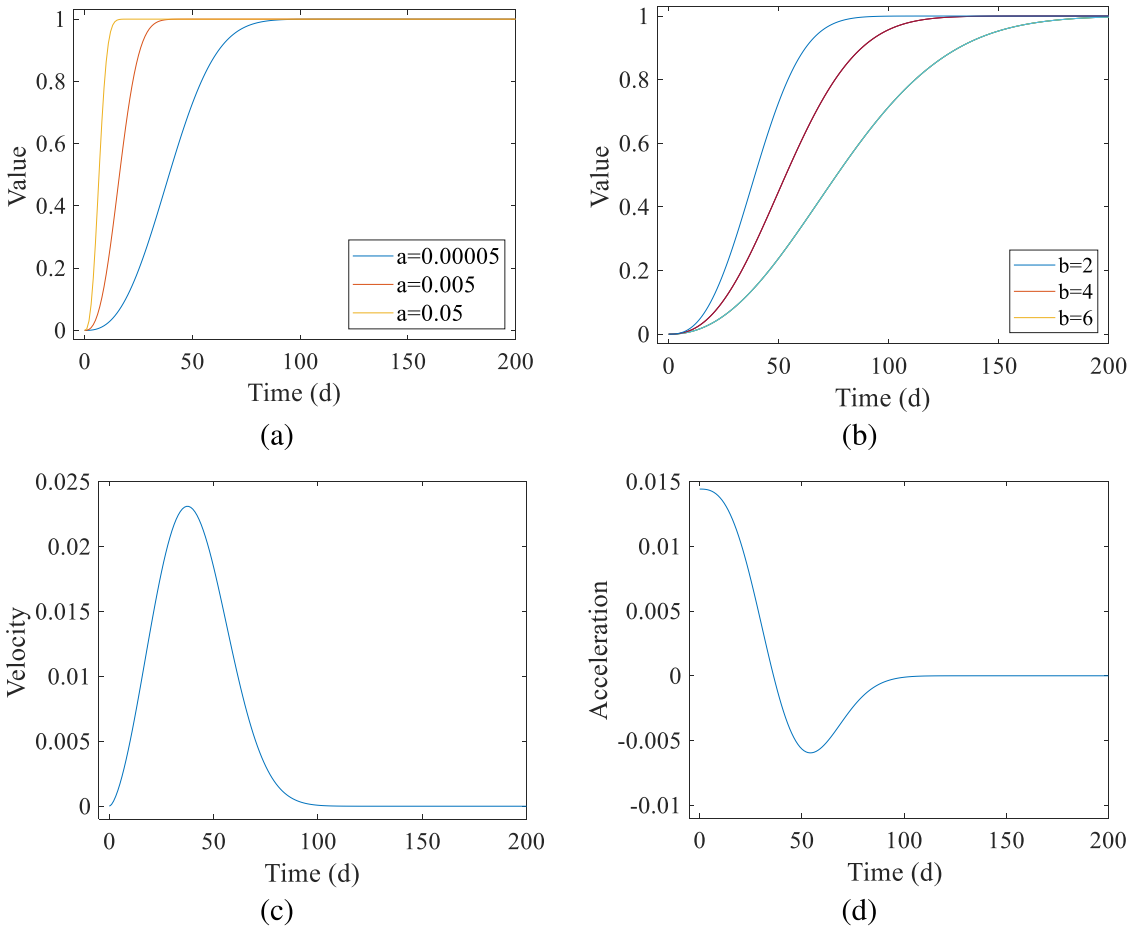

Figure 3. Curve of the weibull function. (a) Relationship between the value curve and parameter *a*; (b) relationship between the value curve and parameter *b*; (c) velocity curve; and (d) acceleration curve.

2.2. Comparison of Advantages of the Improved Threshold Function. The typical time functions commonly used are Knothe time function, Weibull time function, and Compertz time function. Its function-specific expressions are the following.

(1) The expression of the Knothe time function is

$$s(t) = s_{\max} \times (1 - e^{-ct}) \quad (2)$$

where c is the parameter of the time influence function associated with the overburden lithology. The Knothe function curve was plotted using MATLAB software as shown in Figure 2.

In the Knothe time function model, the surface settlement velocity is proportional to the difference between the large settlement value of the surface and the settlement value at a certain moment. With the increase of the value of c taken, the moving deformation of the underground continuous pile caused by the excavation of the foundation pit is more intense and the time required for the deformation to reach a stable state is shorter.[29] Due to the lack of inflection points in the predicted settlement curve, the prediction of settlement velocity and acceleration does not fully comply with the objective fact that the subsurface continuous piles move and deform. However, due to the single parameter and easy access to the measured data or geological conditions, the Knothe time function is still a common functional model for underground space construction.[30]

(2) The expression of the Weibull time function is given by

$$s(t) = s_{\max} \times (1 - e^{-at+b}) \quad (3)$$

where a and b are the model parameters related to the properties of the upper overburden geotechnical layer. Weibull function curves were plotted using MATLAB software as shown in Figure 3.

The curve of the Weibull time function is s-shaped, and the settlement curve starts from the origin and converges to S_m.[31] With the increase of a and b values, the initial period of surface movement is shortened, the convergence time of the surface subsidence curve is longer during the recession period, and the time needed for the inflection point of the subsidence curve is shortened obviously. Under the influence of mining, the degree of surface movement and deformation is more severe. This indicates that the isotropic variation of model parameters a and b has a synergistic effect on the shape of the subsidence curve. In terms of functional expressions, the Weibull time function is actually improved from the Knothe time function. When $b = 1$, the Weibull time function is transformed into the Knothe time function.[32]

(3) The expression of the Gompertz time function is given by

$$s(t) = s_{\max} \times e^{-e^{-at+b}} \quad (4)$$

where a and b are variable morphological parameters, which are related to the mechanical and physical properties of the

https://doi.org/10.1021/acsomega.2c00582
ACS Omega 2023, 8, 23389−23400

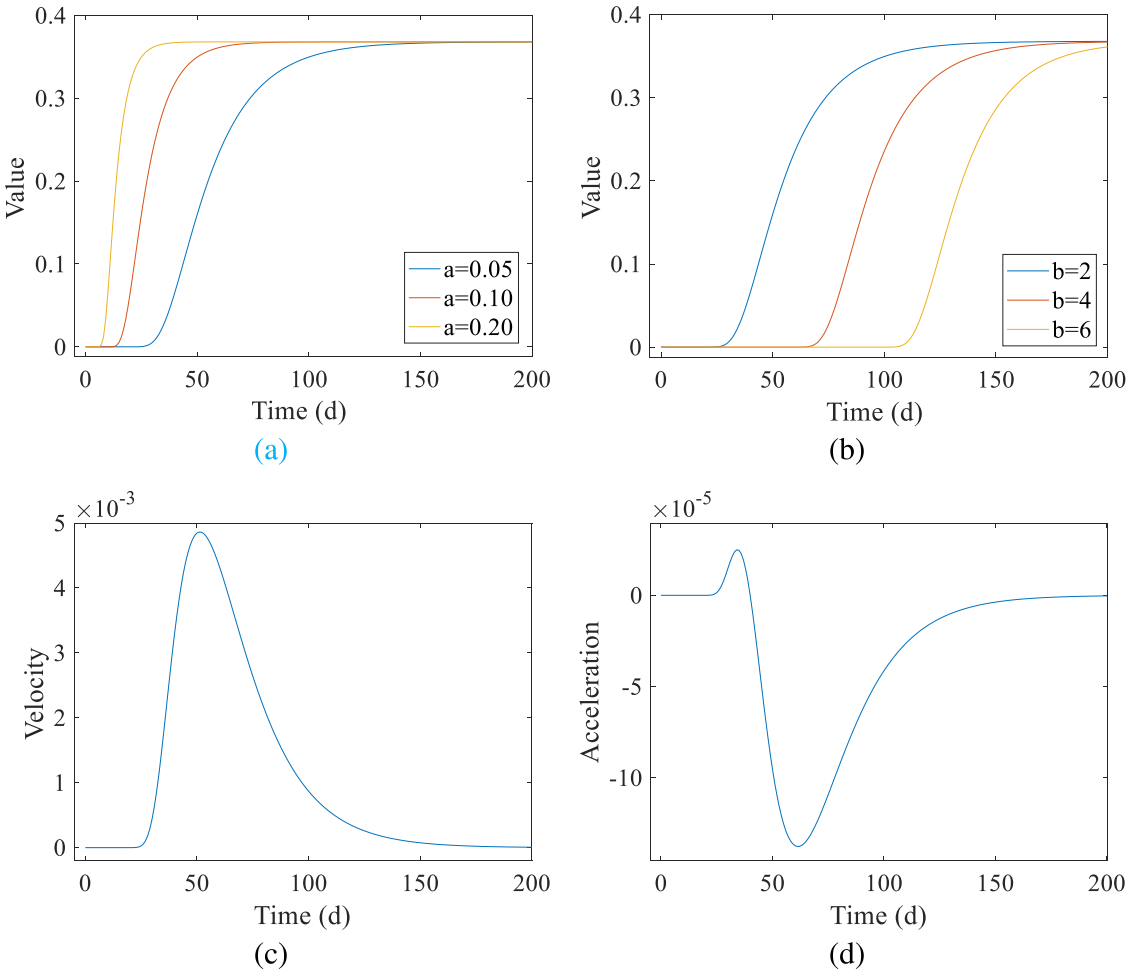

Figure 4. Curve of the Gompertz function. (a) Relationship between the value curve and parameter *a*; (b) relationship between the value curve and parameter *b*; (c) velocity curve; and (d) acceleration curve.

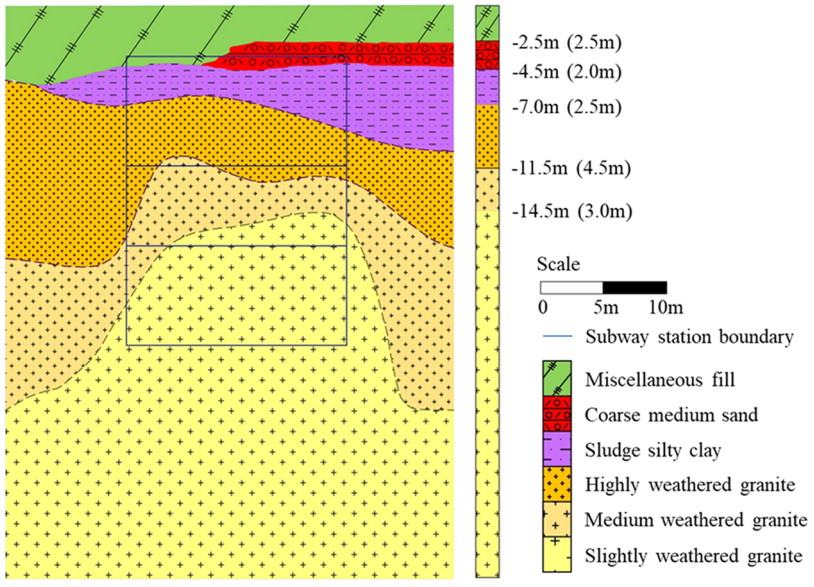

Figure 5. Geological structure surrounding the subway station.

overlying rock in the settlement zone and could affect the geometry of the curve, and *t* is the deformation time. The Gompertz function curve is plotted by MATLAB software, as shown in Figure 4.

The Gompertz time function curve with parameters *a* and *b* can be seen in the graph of the relationship between the Gompertz time function; at the moment $t = 0$, the function value is not 0 but a positive value, which is simply satisfied by

https://doi.org/10.1021/acsomega.2c00582
ACS Omega 2023, 8, 23389−23400

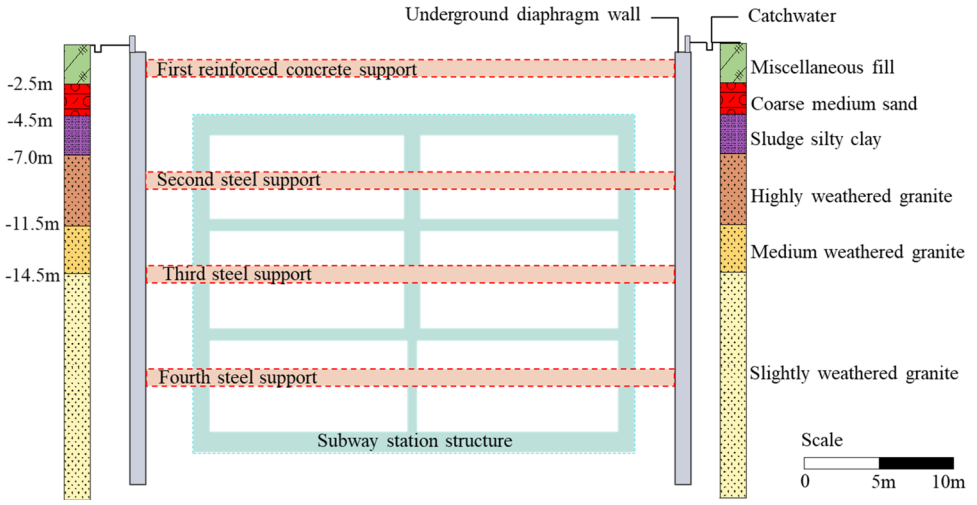

Figure 6. Construction Layout.

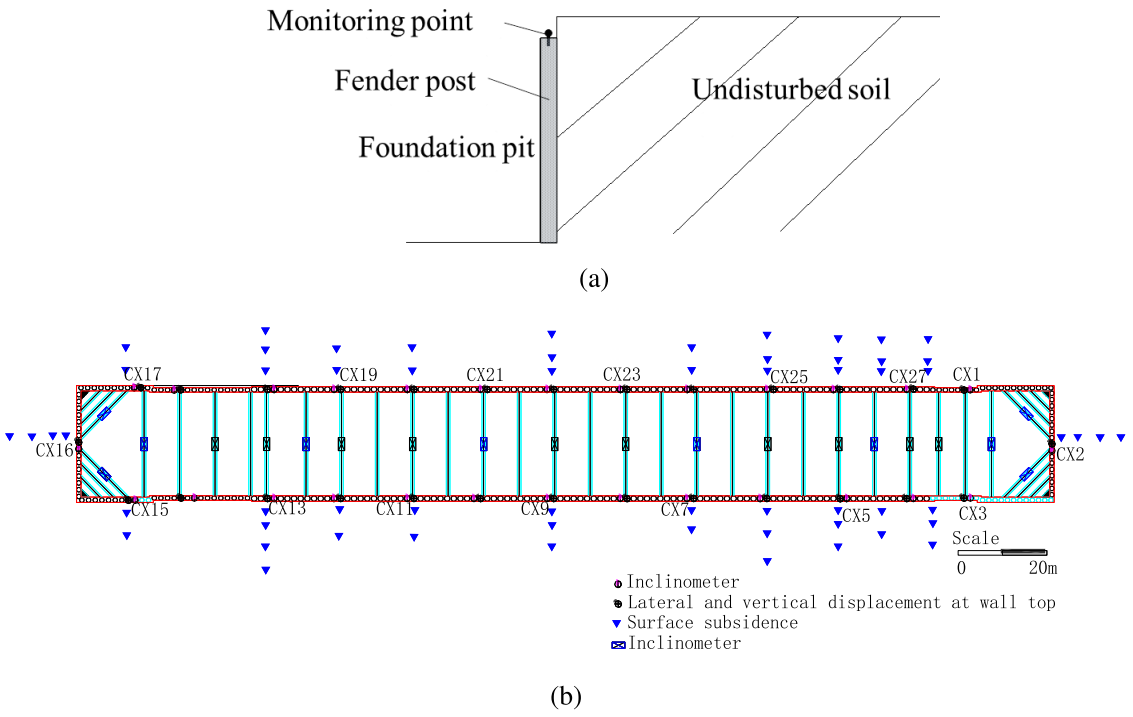

Figure 7. Monitoring point layout map. (a) Diagram of horizontal displacement measurement points on top of the piles. (b) Distribution of monitoring points.

the characteristics of the function value convergence to 1 after the local surface point movement deformation stops. Morphological parameters a and b can be applied to different engineering geological conditions of subsidence. When b is taken as 2, with the increase of a, the slope of the time function curve in the initial period is faster, the time taken for the function value to reach the convergence value 1 is shorter, and when combined with the theory of mining subsidence, it can be seen that the ground point ends the moment of mobile deformation earlier.[33] When a takes 0.05, it is found that the parameter b only controls the path of movement of the function curve and the time used for the function value to reach the final convergence value is basically unchanged, and the larger the parameter b, the later the deformation point reaches the maximum sinking speed.[34]

3. STRUCTURAL STRATIGRAPHY OF THE PIT AND ENCLOSURE SYSTEM

3.1. Project Description. A subway station in Qingdao, Shandong Province, is situated at a "T" intersection on the main road and has a two-storey underground island platform. The station contains four entrances, one fire evacuation door, one pair of ventilation pavilions, and two barrier-free elevators. Its length is 220.1 m, its platform width is 13 m, and its standard portion is 22 m wide. The pit is mostly constructed using the sequential open-cut approach.[35]

https://doi.org/10.1021/acsomega.2c00582
ACS Omega 2023, 8, 23389−23400

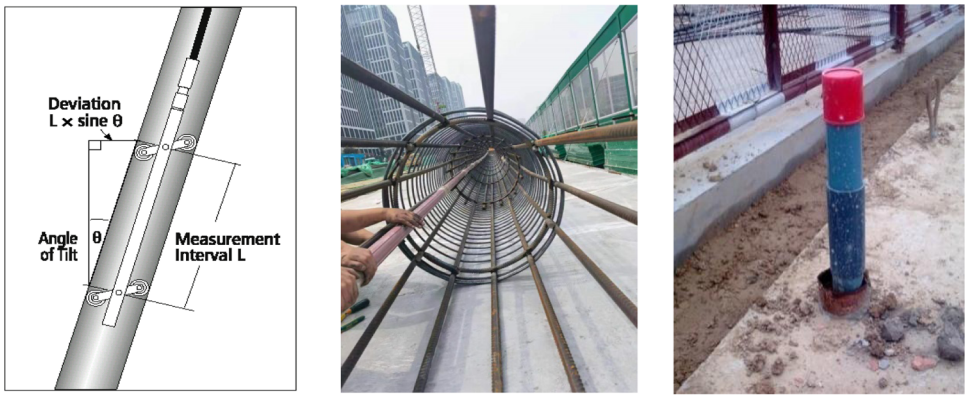

Figure 8. Tilt pipe installation and construction. (a) Schematic diagram of tilt tube measurement principle; (b) schematic diagram of the installation of the tilting pipe; and (c) field picture of the tilting pipe.

3.2. Stratigraphic Structure of the Pit. The stratigraphic structure of the station site from top to bottom is plain fill, medium coarse sand, sludge silty clay, highly weathered granite, highly weathered lamprophyre, medium-weathered granite, and slightly weathered granite, and the station floor is mainly located in medium-weathered granite. Its stratigraphic structure consists of 2.5 m of plain fill, 2 m of coarse medium sand, 2.5 m of sludge silty clay, 4.5 m of highly weathered granite, 3 m of medium-weathered granite, and 26 m of slightly weathered granite. The stratigraphic structure near the foundation pit of this section of the metro station is depicted in Figure 5.

3.3. Main Enclosure System of the Subway Station. The central enclosure system of the station adopts the form of underground enclosure pile enclosure system + internal support system, with a wall thickness of 850 mm and 80 underground enclosure piles for the main enclosure structure. In the normal part of the foundation pit, there are four supports: the first is a concrete support, the second is an 18 mm wide 800 steel support, and the third and fourth are 18 mm thick 600 steel supports.[36]

There are numerous types of utility pipelines within the station's construction area, and a three-story staff dormitory is located 18 m south of the central pit. The profile of the pit is depicted in Figure 6. We use different working conditions to represent different excavation depths and corresponding support measures. The following are the working conditions for excavating the foundation pit.

(1) Condition 1: The first reinforced concrete support was laid at 1.5 m of the pit.
(2) Condition 2:The second steel support was laid at 8.5 m of the pit.
(3) Condition 3: Excavation to 12.5 m, laying the third steel support.
(4) Condition 4: Excavation to 16 m, laying the fourth steel support.
(5) Condition 5: The pit was excavated to 19.6 m at the bottom.

3.4. Monitoring Point Embedment and Observation. *3.4.1. Observation Point Placement.* Drilling boreholes were implemented at the top of the underground diaphragm wall to fix the connecting ribs matched with the prisms, and the prisms were placed on the connecting bars as the horizontal displacement monitoring points at the top of the wall,[37] one every 25 m along the top of the underground diaphragm wall around the foundation pit. The layout monitoring points are shown in Figure 7.

Leica TS11 total station, an angle measurement accuracy of 1″ and distance measurement accuracy of 1.5 mm + 2 ppm, was set up on the forced alignment platform. Two plane control points outside the influence area of the foundation pit were used to measure according to the resection method to obtain the coordinate values of the set up total station measurement points, and then the plane coordinates of each monitoring point on the top of the wall were measured in turn.[38]

3.4.2. Displacement Calculation. The initial monitoring coordinates of each monitoring point on the top of the wall were set as X_0 and Y_0, and the subsequent monitoring values were set as X_n and Y_n. By calculating the difference between the horizontal coordinates of each measuring point and the first coordinates in each period, we can obtain the horizontal displacement of the wall in X and Y directions.

3.5. Underground Enclosure Piles' Internal Horizontal Displacement Monitoring. *3.5.1. Inclinometer Tube Embedded Method.* Observation is carried out by the embedded inclinometer tube, which is fixed on the reinforcement cage of the fender post by direct tying or setting the hoop. The concrete is poured when the reinforcement cage is put into the hole. Each inclinometer tube is arranged with an interval of 20−50 m, and the installation is shown in Figure 8.[39]

3.5.2. Monitoring Method. The horizontal displacement reference point of the enclosure wall is located at the bottom of the inclinometer tube. When the measured pile is deformed, the axis of the inclinometer tube produces deflection, and the horizontal displacement of the pile can be calculated by measuring the inclination angle of each section of the inclinometer tube with the inclinometer.

The monitoring instrument adopts a CX-3C inclinometer, whose main accuracy is ±2 mm/30 m and minimum display is ±0.01 mm/500 mm. When monitoring, the inclinometer probe is put into the bottom inclinometer tube, and then each portion of a length of 0.5 m is tested in succession.[40]

3.5.3. Calculation of Horizontal Movement. The reference point at the bottom of the inclinometer tube is set as point O with coordinates (X_0,Y_0), and the plane coordinates of each

https://doi.org/10.1021/acsomega.2c00582
ACS Omega 2023, 8, 23389−23400

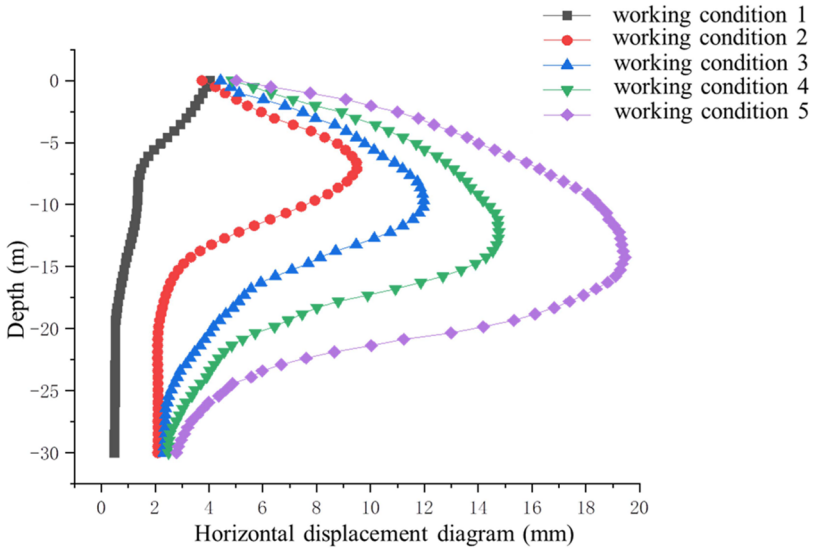

Figure 9. CX13 horizontal displacement diagram for each working condition.

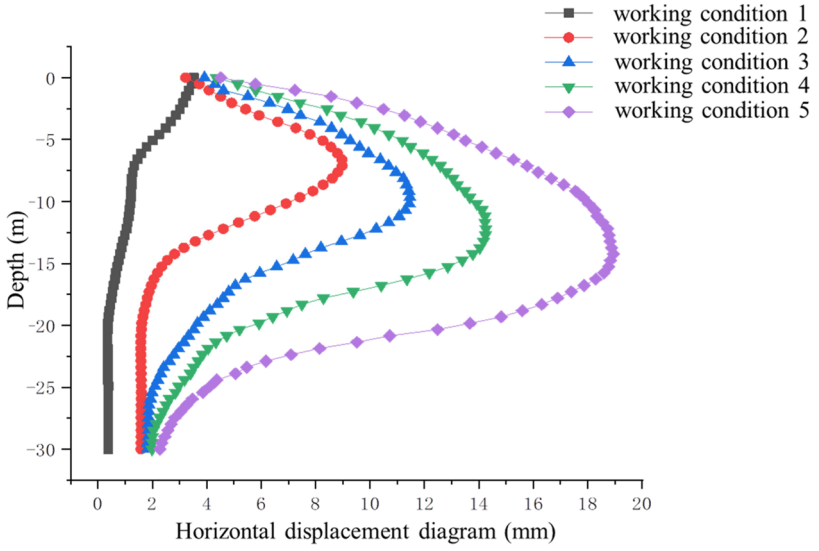

Figure 10. CX07 horizontal displacement diagram for each working condition.

measuring point in the axis of the inclinometer tube are calculated as follows.

$$X_j = X_0 + \sum_{i=1}^{j} L \sin \alpha_{xi} = X_0 + L{\cdot}f{\cdot} \sum_{i=1}^{j} \Delta\varepsilon_{xi} \tag{5}$$

$$Y_j = Y_0 + \sum_{i=1}^{j} L \sin \alpha_{yi} = Y_0 + L{\cdot}f{\cdot} \sum_{i=1}^{j} \Delta\varepsilon_{yi} \tag{6}$$

The plane coordinates of each measuring point in the axis of the measuring inclinometer tube can be calculated by the above equation. Comparing the difference of the horizontal coordinate values of each measuring point in different periods, the horizontal displacement amount in each monitoring period can be obtained for each position inside the wall, and the accumulated horizontal displacement amount of each measuring point can be obtained.[41]

4. RESULTS AND DISCUSSION

4.1. Analysis of Horizontal Displacement of Underground Enclosure Piles. *4.1.1. Relation between Horizontal Displacement and Excavation Depth.* Since the points near the middle of the pit were destroyed, we selected two side sloping pipes, CX07 and CX13, which had more comprehensive monitoring data, for further analysis. Two inclinometer tubes, CX13 and CX07, of the excavated underground diaphragm wall of the subway station pit are selected. There are buildings on one side of point CX13 and no buildings on one side of CX07. The deep horizontal displacement curves of CX13 and CX07 are drawn by Origin software as shown in Figures 5 and 6,[42] and the lateral shift of the wall to the inside of the pit is taken as positive in the figure. The change law of the measured data of the two monitoring points under five different working conditions is analyzed.

As shown in Figures 9 and 10, the trend of the horizontal displacement curve of the two monitoring points is basically the same. At the early stage of foundation excavation, the support is not stable yet, and the displacement of the top of the

https://doi.org/10.1021/acsomega.2c00582
ACS Omega 2023, 8, 23389−23400

Table 1. Parameters of Different Functions

Knothe		Gompertz		Weibull		adjusted-logistic	
parameters	value	parameters	value	parameters	value	parameters	value
S_m	19.30	S_m	19.22	S_m	19.18	S_m	19.30
c	0.009556	a	0.03143	a	4.404×10^{-5}	a	1.2×10^{-5}
		b	2.0880	b	2.2090	b	76.99
						c	3.482

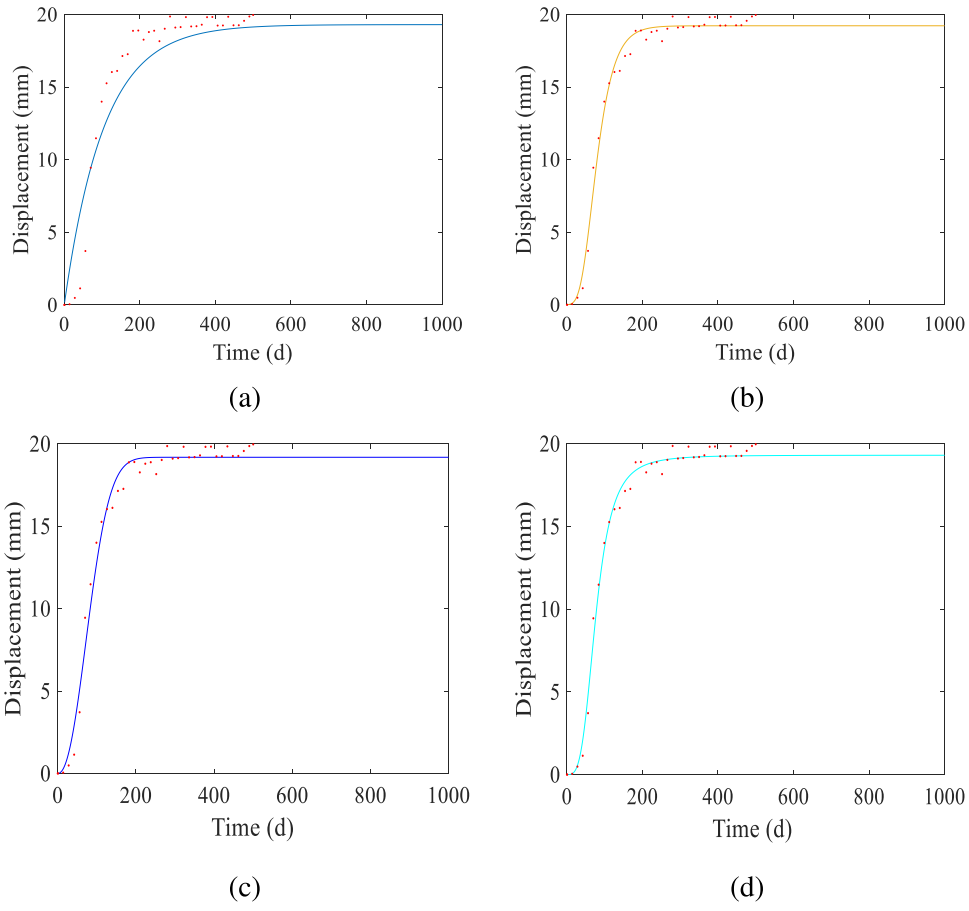

Figure 11. Comparison of measured and predicted values. (a) Knothe time function; (b) Gompertz time function; (c) Weibull time function; and (d) Adjusted-Logistic time function.

underground diaphragm wall is large. Its curve resembles that of a cantilever beam. As the excavation of the foundation pit goes on, the horizontal displacement of the ground connecting wall gradually increases, and the maximum displacement value decreases. In these figures, its shape is similar to a "bow".

The top of the pile of the underground diaphragm wall experiences its maximum horizontal displacement when the pit is excavated to a depth of 2 m, while CX13 and CX07 both get their maximum displacements of 3.5 and 4.02 mm, respectively. When the pit is dug out to a depth of 9 m, the underground diaphragm wall's maximum horizontal displacement is close to 7.0 m, CX13's maximum displacement is 9.5 mm, and CX07's maximum displacement is 9.0 mm. The maximum horizontal displacement of the underground diaphragm wall when the pit is excavated to a depth of 13 m is close to 9.6 m, whereas the maximum displacement of CX13 is 12.0 mm and the maximum displacement of CX07 is 11.5 mm. When the pit is dug out to a depth of 16.5 m, the underground diaphragm wall's maximum horizontal displacement is close to 12.6 m, CX13's maximum displacement is 14.8 mm, and CX07's maximum displacement is 14.3 mm. The greatest horizontal displacement of the underground diaphragm wall occurs when the pit is excavated to the foundation, and it is close to 14.5 m. The maximum displacement of CX13 is 19.5 mm and the maximum displacement of CX07 is 19.0 mm.

When the pit is excavated under the third condition, the horizontal displacement of the underground diaphragm wall increases at a slower rate, so it can be concluded that the third support suppresses the deformation speed of the underground diaphragm wall. When the excavation reaches the bottom of the foundation, the displacement of the underground diaphragm wall increases due to the absence of an enclosure system. With the increase of excavation depth, the maximum horizontal displacement of the underground diaphragm wall gradually decreased and finally stabilized at 0.62−0.71 H.

4.1.2. Prediction Analysis of Horizontal Displacement Deformation. In this paper, a long time series dynamic analysis is made on the historical monitoring data of 18 months. The Adjusted-Logistic time function model, Knothe time function

https://doi.org/10.1021/acsomega.2c00582
ACS Omega 2023, 8, 23389−23400

model, Weibull time function model, and Gompertz time function model were used to fit and predict the historical data. Taking the horizontal displacement data at the maximum horizontal displacement of the CX07 inclined tube as an example, the parameters of different function prediction models are obtained as shown in Table 1.

According to the calculated parameters, the curves of the relationship between horizontal displacement and time predicted by different function models are drawn by MATLAB software, as shown in Figure 11.

The error between the predicted value and the measured value is the standard to evaluate the performance of the model. Therefore, two kinds of error indexes sensitive to data change and the coefficient of determination of goodness of fit are chosen as the evaluation indexes to test the prediction effect. The smaller the root-mean-square error (RMSE) and the mean absolute error, the smaller the error between the predicted value and the measured value and the higher the prediction accuracy. The closer the decisive coefficient R^2 is to 1, the higher the correlation between the regression curve and the measured value and the better the prediction effect. The evaluation indicators are calculated as follows.

(1) Root-mean-square error

$$\mathrm{RMSE} = \sqrt{\frac{1}{n}\sum_{j=1}^{n}[S(t_j) - \hat{S}(t_j)]^2} \tag{7}$$

(2) Mean absolute error

$$\mathrm{MAE} = \frac{1}{n}\sum_{j=1}^{n}|S(t_j) - \hat{S}(t_j)| \tag{8}$$

(3) Coefficient of determination of the goodness of fit

$$R^2 = 1 - \frac{\sum_{j=1}^{n}[S(t_j) - \hat{S}(t_j)]^2}{\sum_{j=1}^{n}[S(t_j) - \overline{S}]^2} \tag{9}$$

The error evaluation indexes of different function models are analyzed statistically, and it is found that the R^2 of Knothe time function model is less than 0.9379, which indicates that the correlation between the Knothe curve and the measured value is low. However, the Adjusted-Logistic time function model's, Gompertz's, and Weibull's R^2 values are all larger than 0.985, indicating that the correlation between the predicted values of the three functions and the measured values is relatively high, which means that they can be used to predict the horizontal displacement of retaining piles. According to the index of prediction precision, the Adjusted-Logistic model has the best prediction precision, followed by the Gompertz time function model, Weibull time function model, and Knothe time function model. Their root-mean-square error is 0.5316, 0.6190, 0.7675, and 1.6649, and their MAE is 0.3752, 0.4497, 0.5694, and 1.0722, respectively, as shown in Table 2.

Table 2. Different Function Model

	Knothe	Gompertz	Weibull	adjusted-logistic
Sm	20.41 mm	19.22 mm	19.18 mm	19.31 mm
RMSE	1.6649	0.6190	0.7675	0.5316
MAE	1.0722	0.4497	0.5694	0.3752
R^2	0.9379	0.9914	0.9870	0.9937

4.2. Building of the Horizontal Cusp Catastrophe Model of the Foundation Pit. In the field data processing, the prediction of deformation trend by the Adjusted-Logistic time function and the dynamic evaluation of pit stability by cusp mutation are combined. First, we use the prediction of the Adjusted-Logistic time function model to screen the abnormal area and then evaluate the stability of the abnormal area by cusp mutation, which can judge the safety state of the foundation pit more effectively.

4.2.1. Building of the Cusp Catastrophe Model. In constructing the cusp catastrophe model[43] of the horizontal displacement cusp of the foundation pit, the polynomial of the time series of the measured deformation values is established based on the real-time data. Here, we take the quadratic polynomial as an example to illustrate the derivation process of the cusp catastrophe model, and the quadratic polynomial fitting function is as follows.[44]

$$U_t = a_0 + a_1 t + a_2 t^2 + a_3 t^3 + a_4 t^4 \tag{10}$$

where U_t is the deformation function, t is the time variable, and a_i is the fitting parameter (i = 0, 1, 2, 3, 4).

The above equation is transformed into the standard form of the catastrophe model by Tschirhaus transformation. By setting $t = x - A$ and $A = a_2/4a_4$, eq 10 could be transformed into eq 11

$$U_x = b_4 x^4 + b_2 x^2 + b_1 x + b_0 \tag{11}$$

where b_i is the fitting parameter (i = 0, 1, 2, 4).

The relationship between the fitting parameters a_i and b_i is shown in eq 12

$$\begin{bmatrix} b_0 \\ b_1 \\ b_2 \\ b_3 \end{bmatrix} = \begin{bmatrix} A^4 & -A^3 & A^2 & -A & 1 \\ -4A^4 & 3A^2 & -A & 1 & 0 \\ 6A^2 & -3A & 1 & 0 & 0 \\ 1 & 0 & 0 & 0 & 0 \end{bmatrix} \begin{bmatrix} a_4 \\ a_3 \\ a_2 \\ a_1 \\ a_0 \end{bmatrix} \tag{12}$$

By dividing eq 11 with b_4 on both sides, the underground diaphragm wall horizontal displacement cusp mutation model standard form can be obtained.

$$U_x = x^4 + ux^2 + vx + c \tag{13}$$

The relationship between the parameters and the fitted parameters are

$$u = \frac{a_2}{a_4} - \frac{3a_2^3}{8a_4^2} \tag{14}$$

$$v = \frac{a_1}{a_4} - \frac{a_2 a_3}{2a_4^2} + \frac{a_3^3}{8a_4^3} \tag{15}$$

A quadratic derivation of the standard form of the mutation theory yields a control threshold, which is

$$\Delta = 8u^3 + 27v^2 \tag{16}$$

According to eq 16, the stability of the underground diaphragm wall deformation could be discriminated: when $\Delta > 0$, the underground diaphragm wall is in a stable state and when $\Delta < 0$, the underground diaphragm wall is in an unstable state. Meanwhile, when the underground diaphragm wall is in a stable state, the smaller the sudden change characteristic value,

https://doi.org/10.1021/acsomega.2c00582
ACS Omega 2023, 8, 23389−23400

Table 3. Monitoring Point Horizontal Displacement Sudden Change Parameters

monitoring point	fitting function	degree of fitting R	catastrophe parameters		
			u	v	Δ
4	$y = -3 \times 10^{-8}x^5 + 4 \times 10^{-6}x^4 - 0.2 \times 10^{-3}x^3 - 0.11 \times 10^{-2}x^2 - 0.197 \times 10^{-1}x - 0.1616$	0.995	−266.7	76,296	1.57×10^{12}
6	$y = 1 \times 10^{-8}x^5 - 2 \times 10^{-6}x^4 + 0.2 \times 10^{-3}x^3 - 0.58 \times 10^{-2}x^2 - 1.199 \times 10^{-1}x + 0.0747$	0.998	2400	216,000	1.37×10^{12}
9	$y = -2 \times 10^{-8}x^5 + 4 \times 10^{-6}x^4 - 0.2 \times 10^{-3}x^3 + 6.6 \times 10^{-3}x^2 - 2.969 \times 10^{-1}x + 0.1885$	0.998	−3600	−164,000	3.53×10^{11}
11	$y = -6 \times 10^{-9}x^5 + 1 \times 10^{-6}x^4 - 0.1 \times 10^{-3}x^3 + 0.77 \times 10^{-2}x^2 - 4.223 \times 10^{-1}x - 0.0388$	0.997	3333.3	−142,963	8.48×10^{11}
16	$y = -2 \times 10^{-8}x^5 + 4 \times 10^{-6}x^4 - 0.3 \times 10^{-3}x^3 + 1.34 \times 10^{-2}x^2 - 4.757 \times 10^{-1}x + 0.1042$	0.998	−600	−60,000	9.55×10^{10}

the better the stability of the underground diaphragm wall and vice versa.

4.2.2. Analysis of the Ground Surface Deformation Cusp Catastrophe Model. Five monitoring points, 4, 6, 9, 11, and 16, which were affected by the excavation of the foundation pit, were selected, and the time series of horizontal displacement deformation rate was monitored during the active period of the underground diaphragm wall deformation. The cusp catastrophe model of each monitoring point was constructed by fitting a quadrinomial, and the parameters and eigenvalues of the model of spike mutation were obtained as shown in Table 3.

According to the deformation rate mutation parameters of each monitoring point calculated in Table 1, the fitting degree of each monitoring point tends to be near 1, which means that the fitting impact is favorable. The catastrophe characteristic value Δ of each monitoring point is greater than 0, which indicates that the underground enclosure piles of the pits are in a stable state and the pits are in a safe state. The catastrophe state parameters of each monitoring point are different, which indicates that there are differences in the stability of the underground enclosure piles of the pit. In summary, the model can achieve the prediction and early warning of the stability of the underground enclosure piles of the subway pit and also has a certain guiding effect on the effective reinforcement of the unstable underground enclosure piles of the pit.

6. CONCLUSIONS

In this paper, the Adjusted-Logistic time function model with three parameters is established, and the theoretical analysis shows that the Adjusted-Logistic time function can adjust the deformation velocity and deformation acceleration in different stages and can predict the "asymmetric time curve". Furthermore, the horizontal displacement values of the underground enclosure piles under different mining depths are calculated by using the monitoring data obtained from the total station and inclinometer. The relationship between the internal displacement of the wall and the excavation depth of the foundation pit is determined. With the excavation depth increasing, the maximum horizontal displacement of the underground enclosure piles finally stabilizes at 0.62−0.71 H. At the same time, the Adjusted-Logistic function model was used to fit and predict the field data. It was found that the RMSE, MAE, and R^2 were 0.5316, 0.3752, and 0.9937, respectively. Finally, the catastrophe model of the horizontal displacement cusp of the foundation pit is established, and the stability of the underground enclosure piles is evaluated by using the measured displacement data, which provides a technical basis for effective reinforcement and treatment of the foundation pit.

AUTHOR INFORMATION

Corresponding Author

Hengxuan Luan − *College of Mechanical and Electronic Engineering, Shandong University of Science and Technology, Qingdao 266590, China; China Coal Electric Co., Ltd., Beijing 101300, China*; Email: hengxuanluan@163.com

Authors

Yue Dong − *College of Geodesy and Geomatics, Shandong University of Science and Technology, Qingdao 266590, China*; orcid.org/0000-0002-5635-0849

Yuanzhong Luan − *College of Geodesy and Geomatics, Shandong University of Science and Technology, Qingdao 266590, China*

Fei Wang − *College of Geodesy and Geomatics, Shandong University of Science and Technology, Qingdao 266590, China; Shandong Branch of China National Geological Exploration Center of Building Materials Industry, Jinan 250000, China*

Huilong Yang − *China Coal Electric Co., Ltd., Beijing 101300, China*

Zheng Jia − *College of Geodesy and Geomatics, Shandong University of Science and Technology, Qingdao 266590, China*

Complete contact information is available at: https://pubs.acs.org/10.1021/acsomega.2c00582

Notes

The authors declare no competing financial interest.

ACKNOWLEDGMENTS

This study was supported by the National Natural Science Foundation of China (Grant No. 52204171), the China Postdoctoral Science Foundation (2021M693546), the Shandong Provincial Natural Science Foundation (ZR2020MD024, ZR2021QE085), the Youth Innovation Team Development Program of Higher Education Institutions of Shandong Province (2022KJ321), and the Open Research Fund of Key Laboratory of Jinan Digital Twins and Intelligent Water Conservancy (37H2022KY040114).

REFERENCES

(1) Luo, C.; Cheng, Y.; Bai, Z.; et al. Study on Settlement and Deformation of Urban Viaduct Caused by Subway Station Construction under Complicated Conditions. *Adv. Civ. Eng.* **2021**, *2021*, 1−16.

(2) Zhong, Z. Comparison of foundation pit optimization schemes of cross oblique transfer station. *J. Archit. Civ. Eng.* **2023**, *40*, 150−158.

(3) Zhang, A.; Mo, H. Analytical solution for pile response due to excavation-induced lateral soil movement. *J. Inf. Comput. Sci.* **2014**, *4*, 1111−1120.

https://doi.org/10.1021/acsomega.2c00582
ACS Omega 2023, 8, 23389−23400

(4) Li, Y.; Zhang, W.; Zhang, R. Numerical investigation on performance of braced excavation considering soil stress-induced anisotropy. *Acta Geotech.* **2022**, *2*, 563−575.
(5) Li, S.; Zhang, D.; Shao, Y. Analysis of soil displacement fields outside deep excavations in composite deformation model of Beijing subway station. *J. Beijing Jiaotong Univ.* **2020**, *44*, 13−23.
(6) Li, Y.; Wang, C.; Sun, Q.; Xing, Y. Influence of subway deep foundation excavation on surrounding ground settlement. *J. Liaoning Tech. Univ.* **2017**, *36*, 387−390.
(7) Ran, Q.; Wang, X.; Wang, B.; et al. Model tests on influences of excavation of foundation pits on bending moment and deformation of pile foundation of adjacent buildings. *J. Geotech. Eng.* **2021**, *43* (S1), 132−137.
(8) Sun, C.; Xu, C. J. Influence of Excavation of a Deep Excavation on the Surrounding Environment. *J. Jilin Univ., Earth Sci. Ed.* **2019**, *49*, 1698−1705.
(9) Feng, Z.; Xu, Q.; Xu, X.; et al. Deformation Characteristics of Soil Layers and Diaphragm Walls during Deep Foundation Pit Excavation: Simulation Verification and Parameter Analysis. *Symmetry* **2022**, *14*, No. 254.
(10) Li, Z. Displacement Monitoring during the Excavation and Support of Deep Foundation Pit in Complex Environment. *Adv. Civil Eng.* **2021**, *2021*, 1−7.
(11) Peck, R. B.; Terzaghi, K.; Middlebrooks, T. A.; et al. Discussion of "Peck on Levee Failure". *Trans. Am. Soc. Civ. Eng.* **1944**, *109*, 1414−1426.
(12) Ou, C.; Hsieh, P.; Chiou, D. Characteristics of ground surface settlement during excavation. *Can. Geotech. J.* **1993**, *30*, 758−767.
(13) Qin, F.A.; Hu, Z.-X.; Peng, S.-J. Depth of soil stabilization in passive area of foundation pits for shanghai soft clay. *Chin. J. Geotech. Eng.* **2008**, *30*, 935−940.
(14) Xu, Z. *Deformation Behavior of Deep Excavations Supported by Permanent Structure in Shanghai Soft Deposit*; Shanghai Jiao Tong University: Shanghai, 2007.
(15) Yang, B.; Zhong, X. Numerical analysis of deep excavation on FLAC-3D. *J. Hebei Univ. Eng., Nat. Sci. Ed.* **2008**, 15−18.
(16) Liao, S.; Wei, S.; Tan, Y. Field performance of large-scale deep excavations in Suzhou. *Chin. J. Geotech. Eng.* **2015**, *37*, 458−469.
(17) Liu, M. *Research on Design Method of Foundation Pit Support System of Subway Station Based on the Strata Deformation Control*; Beijing Jiaotong University: Beijing, 2018.
(18) Liu, H.; Li, K.; Wang, J.; Cheng, C. Numerical Simulation of Deep Foundation Pit Construction under Complex Site Conditions. *Adv. Civil Eng.* **2021**, *2021*, 1−11.
(19) Zhang, Y.; Wu, W.; Jiang, G.; et al. A new approach for estimating the vertical elastic settlement of a single pile based on the fictitious soil pile model. *Comput. Geotech.* **2021**, *134*, No. 104100.
(20) Knothe, S. Time influence on a formation of a subsidence surface. *Arch. Gorn. Hutn.* **1952**, *1*, 1−2.
(21) Zhang, B.; Cui, X. Optimization of segmented Knothe time function model for dynamic prediction of mining subsidence. *Rock Soil Mech.* **2017**, *38*, 541−548.
(22) Yu, C.; Zhao, L.; Li, M.; et al. Prediction of surface progressive subsidence and optimization of predicting model parameters based on the Logistic time function. *J. Saf. Environ.* **2020**, *20*, 2202−2210.
(23) Liu, Y.; Liu, S.; Liu, Y. Discussion on some time functions for describing dynamic course of surface subsidence due to mining. *Rock Soil Mech* **2010**, *31*, 925−931.
(24) Xu, H.; Liu, X. Time function of surface subsidence based on logistic growth model. *Rock Soil Mech.* **2005**, *26*, 151−153.
(25) Xi, G.; Hong, X.; Shao, H. Application of Improved Logistic Function Model to Prediction of Surface Subsidence. *Coal Sci. Technol.* **2013**, *41*, 114−117.
(26) Li, C.; Zhao, L.; Li, M.; et al. Prediction of surface progressive subsidence and optimization of predicting model parameters based on the Logistic time function. *J. Saf. Environ.* **2020**, 2202−2210.
(27) Li, C.; Ding, L.; Cui, X.; et al. Calculation Model for Progressive Residual Surface Subsidence above Mined-Out Areas Based on Logistic Time Function. *Energies* **2022**, *15*, No. 5024.
(28) Wang, J.; Yang, K.; Wei, X.; et al. Prediction of Longwall Progressive Subsidence Basin Using the Gompertz Time Function. *Rock Mech. Rock Eng.* **2022**, *55*, 379−398.
(29) Zhang, L.; Chen, H.; Yao, Z.; et al. Application of the Improved Knothe Time Function Model in the Prediction of Ground Mining Subsidence: A Case Study from Heze City, Shandong Province, China. *Appl. Sci.* **2020**, *10*, No. 3147.
(30) Guo, X.; yang, X.; Chai, S. Optimization of the segmented Knothe function and its dynamic parameter calculation. *Rock Soil Mech.* **2020**, *41*, 2091−2097.
(31) Qu, G.; Zheng, M.; Wang, X.; et al. A freeze−thaw damage evolution equation and a residual strength prediction model for porous concrete based on the Weibull distribution function. *J. Mater. Civil Eng.* **2023**, *5*, No. 04023074.
(32) Li, Y.; Zhang, F.; Hu, L.; et al. Distinct element modelling of mining-induced instability of a heterogeneous fault. *Bull. Eng. Geol. Environ.* **2023**, *82*, No. 69.
(33) Wang, J.; Yan, L.; Yang, K.; et al. Deriving Mining-Induced 3-D Deformations at Any Moment and Assessing Building Damage by Integrating Single InSAR Interferogram and Gompertz Probability Integral Model (SII-GPIM). *IEEE Trans. Geosci. Remote Sens.* **2022**, *60*, 1−17.
(34) Wang, J.; Yang, K.; Wei, X.; et al. Prediction of Longwall Progressive Subsidence Basin Using the Gompertz Time Function. *Rock Mech. Rock Eng.* **2022**, *55*, 379−398.
(35) Zhou, X.; Wang, J.; Mao, L.; et al. Design of typical subway station structure and its enclosure with open cut method in Chengdu city. *Appl. Mech. Mater.* **2014**, *501-504*, 1711−1714.
(36) Lu, L.; Sun, H.; Wang, G.; et al. Deformation of Deep Foundation Pit Combining Support and Main Structure in Subway Station. *China Railway Sci.* **2021**, *42*, 9−14.
(37) Zhou, J.; Xiao, H.; Jiang, W.; et al. Automatic subway tunnel displacement monitoring using robotic total station. *Measurement* **2020**, *151*, No. 107251.
(38) Ma, G. *The Research of Total Station Automatic Monitoring System's Construction and Application on the Subway*; Liaoning Technical University: Fuxin, 2014.
(39) Li, J.; Song, Y.; Wen, M. Research of Improved Installation Methods of Fixed Inclinometer. *J. Changjiang Inst. Technol.* **2012**, *29*, 10−12.
(40) Ren, Q.; Zhang, G.; Yue, X.; et al. Deep foundation pit monitoring based on CX-3C inclinometer. *Appl. Mech. Mater.* **2014**, *484−485*, 404−407.
(41) Malarski, R.; Nagórski, K.; Woźniak, M. Application of Inclinometer Measurements for Relative Horizontal Displacement Investigations on Landslide Grounds. *Rep. Geod. Geoinf.* **2013**, *94*, 6−13.
(42) Chang, B.; Liu, S.; Han, J. Application of Origin Software to Analyzing Deformation Monitoring Data during the Construction of Tunnel. *J. Chongqing Jiaotong Univ., Nat. Sci.* **2008**, 221−224.
(43) Xue, Y.; Wang, D.; Li, S.; et al. A risk prediction method for water or mud inrush from water-bearing faults in subsea tunnel based on cusp catastrophe model. *KSCE J. Civil Eng.* **2017**, *21*, 2607−2614.
(44) Belousov, A. V.; Belyanov, A. A.; Chernyaev, A. P. Errors in fitting radial dose function of cobalt sources for brachytherapy with 3-5 degree polynomials. *Almanac Clin. Med.* **2016**, *44*, 140−147.

https://doi.org/10.1021/acsomega.2c00582
ACS Omega 2023, 8, 23389−23400